2011 JAN 24

Liquid-Air Transpired Solar Collector: Model Development and Sensitivity Analysis

Abdul Qadir
Graduate Student, Masdar Institute of Science and Technology
Abu Dhabi, United Arab Emirates

Peter R. Armstrong
Associate Professor, Masdar Institute of Science and Technology
Abu Dhabi, United Arab Emirates

ABSTRACT

The paper develops a numerical model of a novel hybrid liquid-air transpired solar collector which could simultaneously heat air and water. An energy balance is performed, leading to a system of ODEs which is solved to obtain the air and water outlet temperatures of the collector. Three sets of sensitivity analyses have been performed on the collector varying the total thermal capacitance of the air and water$(\dot{m}c_p)_{total}$, air capacitance rate fraction $R_{\dot{m}cp}$, water inlet temperature T_{wi}, ambient temperature T_{amb}, solar radiation G and wind speed V_w. General performance curves for the collector with increasing $(T_{wi}-T_{amb})/G$ have been developed as a result of these analyses. It is noticed that a $R_{\dot{m}cp}$ between 0.3 and 0.4 provides the highest collector performance. At low $R_{\dot{m}cp}$, collector performance becomes sensitive to wind speed. Lastly it has been shown that the Hottel- Whillier equation is a reasonable approximation for the collector when the radiation loss term is linearized.

INTRODUCTION

Over 60% of peak electricity usage in Abu Dhabi city is accounted due to cooling[1]. This, coupled with the high solar resource[2], encourages the use of solar energy towards cooling applications. The city of Abu Dhabi has a very humid climate, where summer time humidity ratios go up to 25.2 g/kg[2]. It has been proposed that latent loads can be economically addressed by thermally regenerated desiccant cycles[3]. This allows for the separation of latent and sensible cooling functions and thus higher chilled water temperatures may be used to handle the sensible cooling load, decreasing the energy input to a vapor compression chiller[4]. Moreover absorption chillers designed to operate at higher chilled water temperatures have higher COP than those at lower chilled water temperatures[3].

Solar energy can be incorporated in the regeneration of liquid desiccants and some of the regenerated liquid can be stored for use at night. Previously there have been studies towards the use of flat plate collectors and transpired solar collectors in desiccant regeneration applications[5]. However the use of both glazed and unglazed flat plate collectors as well as transpired collectors has proved economically unfeasible [6]. The transpired and unglazed liquid collectors exhibit low efficiencies when heating air and water respectively to a regeneration temperature of 70^{o}C while glazed flat plate collectors have higher efficiencies but are significantly more expensive.

This paper formulates the steady state model of a potentially economical and efficient unglazed, liquid-air transpired solar collector (LATSC) that simultaneously heats water and ambient air. We postulate that this type of collector could be especially useful for desiccant regeneration because the regeneration process needs a continuous supply of fresh air to carry away vapor released when the weak LiBr solution is heated moderately to a temperature below its bubble point. Thus the heat gain of the LATSC suction air (whose main purpose in this application is suppression of convection loss) can be put to good use in the desiccant regeneration process.
Using a steady-state finite difference model we explore the sensitivity of LATSC collection efficiency to variations in air and water flow rate, water inlet temperature, and ambient conditions of temperature, incident solar irradiation, and wind speed.

NOMENCLATURE

A	Collector area (m^2)
c_{pa}	Specific heat of air (kJ/kgK)
c_{pw}	Specific heat of water (kJ/kgK)
D_h	Hole diameter
e_{hx}	Heat exchange effectiveness of perforated plate
F	Fin efficiency
F’	Collector efficiency factor

F_R Collector heat removal factor for water
G Incident solar radiation (W/m^2)
k Thermal conductivity (W/mK)
L Length of collector (m)
L_c Characteristic length of collector (m)
$(\dot{m}c_p)_{total}$ Total thermal capacitance rate of air and water
$\dot{m}_a$ Mass flow rate (kg/s)
$R_{\dot{m}cp}$ Ratio of $\dot{m}c_{p_{air}}$ to $\dot{m}c_{p_{total}}$
Nu Nusselt's number
NTU Number of transfer units
P Perimeter of plenum cross section (m)
Pitch Spacing of holes on absorber plate (m)
$q_{conv,loss}$ Convection loss per unit area(W/m^2)
$q_{rad,loss}$ Radiation loss per unit area (W/m^2)
$q_{c,air}$ Heat transferred to suction air per unit area (W/m^2)
Q_u Useful energy transferred to water (W)
Re Reynold's Number
sep Distance between tubes in absorber
$T_a(y)$ Air temperature (K)
T_{amb} Ambient temperature (K)
$T_m(y)$ Mean of plate and sky temperature (K)
$T_{pl}(y)$ Plate temperature (K)
T_{sky} Sky Temperature (K)
$T_w(y)$ Water Temperature (K)
U_a Heat transfer coefficient for air behind collector (W/m^{2}K)
U_l Total top loss coefficient (W/m^{2}K)
U_d Heat transfer coefficient of air through perforations
U_{wind} Heat transfer coefficient to wind
V_s Suction face velocity
V_w Wind Speed
W Width of collector (m)
x lateral distance from tube
y distance from inlet end of collector

Greek letters:

ϵ Emissivity of collector plate
ρ Density (kg/m^3)
μ Dynamic viscosity (m^2/s)
σ Stephan-Boltzmann constant

Subscripts:

a air
d pertaining to air flowing through perforations
exit exit from the perforations
i inlet
o outlet
tot air +water
w water

MODEL FORMULATION

The collector profile is that of a fin tube flat plate collector in which the plate used is perforated in the manner of a conventional transpired solar collector[7, 8]. Thus water is heated in tubes that run from the base of the collector to the top where it exits via a standard header tube, while the air is sucked through the plate and heated as it travels behind the plate from a given point of entry to the top where it exits via an air duct. A sketch of the collector is shown in figure 1.

The energy balance on a differential element of the collector with unit width is shown in figure 2.

The energy balances for water and air respectively are:

$$\dot{m}_w c_{pw} \frac{dT_w}{dy} = Q_u \quad (1)$$

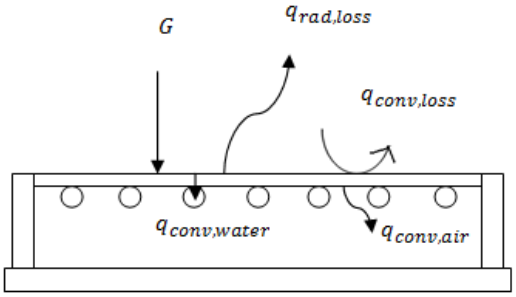

Figure 1: Sketch of end view of collector

$$(\dot{m}_{ai} + \Delta\dot{m}_a)\frac{dT_a}{dy} = \frac{\dot{m}_{a,tot}}{L}[(1 - e_{hx})T_{amb} + e_{hx}T_{pl} - T_{ai}] \quad (2)$$

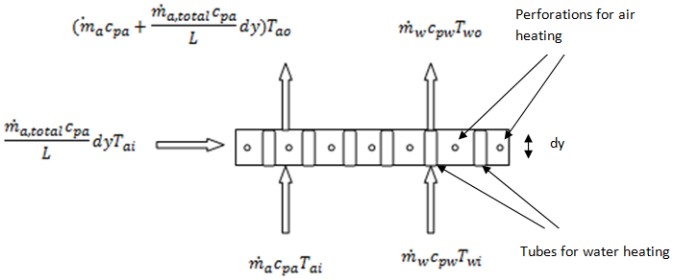

Figure 2: Differential element of the collector in plan view

The mass balance for air entering each element of the collector is:

$$\frac{d\dot{m}_a}{dy} = \frac{\dot{m}_{a,total}(y)}{L} \quad (3)$$

The expressions for e_{hx} and Q_u are developed below.
In the above expressions, e_{hx} is the heat exchange effectiveness of the perforated plate and is calculated by the following correlations developed by Kutscher:

$$Re_d = \frac{V_s D_h}{por * \mu} \quad (4)$$

$$Nu_d = 2.75\left(\left(\frac{pitch}{D_h}\right)^{-1.21} {Re_d}^{0.43} + 0.011por * Re_d \left(\frac{V_w}{V_s}\right)^{0.48}\right) \quad (5)$$

$$U_d = \frac{Nu_d k_a}{D_h} \quad (6)$$

$$V_s = \frac{\dot{m}_a}{\rho_a A} \quad (7)$$

$$NTU = (1 - \sigma(1 - \frac{D_t}{sep}))U_d \quad (8)$$

$$e_{hx} = 1 - \exp(-NTU) \quad (9)$$

Furthermore we require the plate temperature T_{pl} and heat transferred to the water Q_u in order to solve the derived ODEs. In order to obtain these we account for the convective and radiative heat losses from the top of the plate obtained from literature.

Firstly we tackle the convective heat loss due to wind which is sensitive to air face velocity (Kutscher) according to:

$$q_{conv,loss} = U_{wind}(T_{pl} - T_{amb})) \quad (10)$$

Where,

$$U_{wind} = 0.82\frac{V_w \mu_a \rho_a c_{pa} k_a}{V_s L L_c} \quad (11)$$

Then we account for the heat loss due to radiation:

$$q_{rad,loss} = \epsilon\sigma 4{T_m}^3(T_{pl} - T_{sky}) \quad (12)$$

Where

$$T_m = (T_{pl} + T_{sky})/2 \quad (13)$$

We can also express the heat transferred to the air as it passes through the perforations as a convective heat loss from the plate.

$$q_{c,air} = \dot{m}_a c_{pa} e_{hx} \frac{(T_{pl} - T_{amb})}{A} \quad (14)$$

Thus an overall heat "loss" coefficient, U_l, can be expressed as the sum of convective and radiative heat losses with respect to $(T_{pl}-T_{amb})$.

$$U_l = \frac{q_{rad,loss} + q_{c,air} + q_{conv,loss}}{(T_{pl} - T_{amb})} \quad (15)$$

Thus we can now derive the total energy transferred to the water at each element by performing an energy balance on that element using U_l[9].

$$Q_u = W * dy * (G - U_l(T_{pl} - T_{amb})) \quad (16)$$

As the plate temperature varies in both the x and y direction, it is useful to express Q_u in terms of the fluid inlet temperature T_{fi}:

$$Q_u = W * dy * F'(G - U_l(T_{fi} - T_{amb})) \quad (17)$$

Where F' is the collector efficiency factor which accounts for thermal resistances between various points on the plate and the cooling water. Part of the resistance is due to fin efficiency, F, of the collector plate. These factors are given by:

$$F' = \frac{\frac{1}{U_l}}{sep(\frac{1}{U_l(D_t + (sep - D_t)F)} + \frac{1}{C_b} + \frac{1}{\pi D_t h_{fi}})} \quad (18)$$

where

$$F = \frac{tanh * m\frac{sep - D_t}{2}}{m\frac{sep - D_t}{2}} \quad (19)$$

and

$$m = \sqrt{\frac{U_l}{k_p \delta}} \quad (20)$$

Uncoupled Model

The model derived so far does not take in to account the heating of air behind the collector plate as the air moves up the collector towards the outlet. We call this the uncoupled model.

In this model, for a finite air flow rate, a uniformly porous plate will produce a laminar boundary layer that is continuously replenished from the plate and thus completely suppresses convective coupling with the cooler air that is already moving through the channel.

In order to accurately calculate the heating of the air behind the plate(coupled heating) a correlation is needed which accounts for the fact that while the air behind the plate has some contact with the plate, there is also an injection of air through the plate which may limit complete contact with the plate. Figure 3 demonstrates the flow of air behind the collector with the injection of air in to the airstream due to the suction at the front side of the collector plate.

The case where there is no heating of air behind the plate provides a lower limit for the air outlet temperature and upper limit of the water outlet temperature.

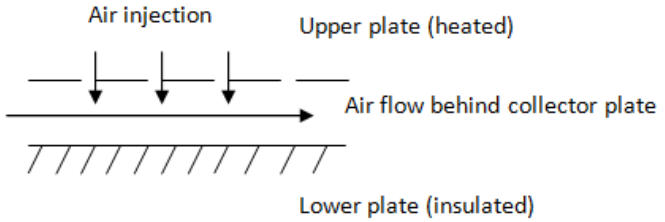

Figure 3: Air flow behind the collector plate.

Coupled Model

On the other hand if it is assumed that there is no boundary layer replenishment by air through the plate and that the flow behind the collector is laminar with uniform heat flux from the

plate and the back wall insulated, we can obtain a model which will provide the upper limit of the air outlet temperature and lower limit of the water outlet temperature. For this model it is assumed that the air flowing behind the collector is laminar and the width of the collector is considerably larger than the plenum depth. The Nusselt number for such a flow is 5.39[10]. Thus U_a is calculated as:

$$U_a = \frac{Nu_D k_{air}}{D_H} \quad (21)$$

Where

$$D_H = \frac{4A}{P} \quad (22)$$

The heat transferred to the air behind the collector is thus:

$$q_{back} = U_a * (T_{pl} - T_{ai}) \quad (23)$$

For the uncoupled model, the 'loss' term of (23) is added to the numerator in equation (15) to account for the heat extracted from the plate. Furthermore q_{back} is also added to the right hand side of equation (2) in order to obtain the energy balance for the air.

The two energy balance equations(1&2) and the mass balance equation(3) were then solved simultaneously using the forth/fifth order Runge-Kutta method in the computation software Matlab™[11].
Thus by solving these equations, the outlet air and water temperature through the collector and consequently the efficiency of the collector are obtained for the models with and without heating of the air behind the collector plate.

SENSITIVITY ANALYSIS

With the foregoing collector model we can observe the performance sensitivity of the collector to varying the ambient temperature(T_{amb}), inlet water temperature(T_{wi}), collector emissivity(ϵ) and total thermal capacitance of air and water($(\dot{m}c_p)_{total}=\dot{m}_w c_{pw} + \dot{m}_a c_{pa}$). Moreover for each analysis, the ratio of thermal capacitance of air to total thermal capacitance ($R_{\dot{m}cp}$) was varied to observe the effect it had on the efficiency of the collector along with the other varying parameters. Throughout the analysis, the collector dimension, air properties, weather condition and solar radiation have been held constant at values specified in Table 1.

Table1: Geometric parameters, fluid properties and baseline conditions used in the sensitivity analysis

Property	**Value**
Solar radiation (S)	800W/m^2
Wind speed(V_w)	3 m/s
Air temperature(Tamb)	25 ^{o}C
Air density(ρ_a)	1.184kg/m^3
Air Viscosity (μ_a)	1.849*10^{-5} Ns/m^2
Air Cp (c_{pa})	1.007kJ/kgK
Length of collector (L)	2m
Width of collector (W)	1m
Plenum depth (D)	0.1m
Perimeter of plenum cross section	2.2m
Plate absorptivity	0.9
Plate emissivity	0.9
Hole diameter	0.025m
Hole pitch (triangular pattern)	0.00159m

The first analysis was aimed at obtaining the performance of the collector with different $(\dot{m}c_p)_{total}$ entering the collector along with a range of values of $\dot{m}c_{p\ ratio}$ from 0.1 to 0.9. The range of values of $(\dot{m}c_p)_{total}$ was from 5W/m^{2}K to 25W/m^{2}K at five equal intervals and the ambient temperature was maintained at =25^{o}C. The results obtained for these analyses are shown in figure 3 and 5 for the model without heating the air behind the collector plate and in figure 4 and 6 when air is heated behind the collector plate.

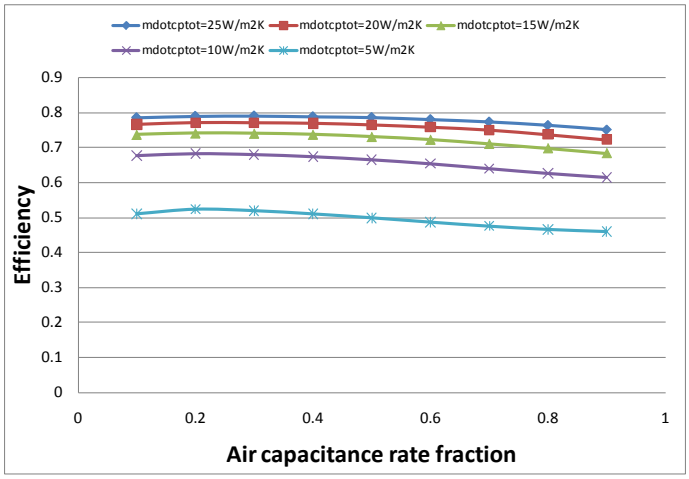

Figure 3: Efficiency vs. $R_{\dot{m}cp}$for range of $(\dot{m}c_p)_{total}$ with $T_{w,i}$ = T_{amb} = 25°C uncoupled air heating.

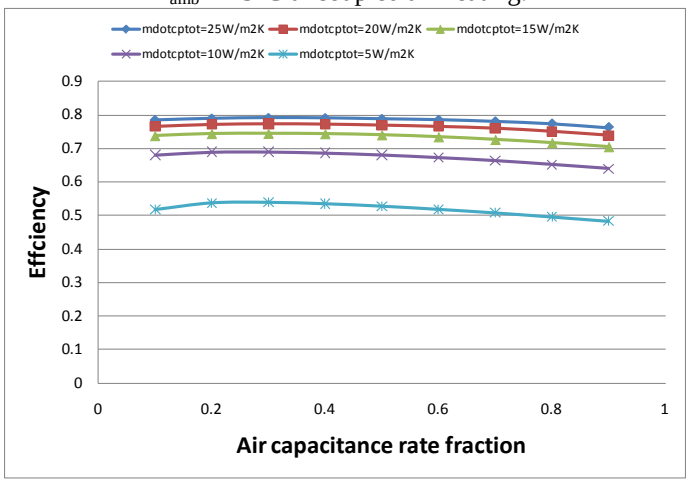

Figure 4: Efficiency vs. $R_{\dot{m}cp}$ for range of $(\dot{m}c_p)_{total}$ with $T_{w,i}$ = T_{amb} = 25°C for coupled air heating.

The second set of analysis was performed by varying the inlet temperature of the water from 25°C to 115°C to obtain the efficiency of the collector. The ambient temperature for this analysis was fixed at 25°C and the $(\dot{m}c_p)_{total}$ was fixed at 15W/m^{2}K. The emissivity and $R_{\dot{m}cp}$ was also varied to obtain a family of curves for emissivities and $R_{\dot{m}cp}$ s of 0.1, 0.5 and 0.9. The results are shown in figures 7, 8 and 9 respectively.

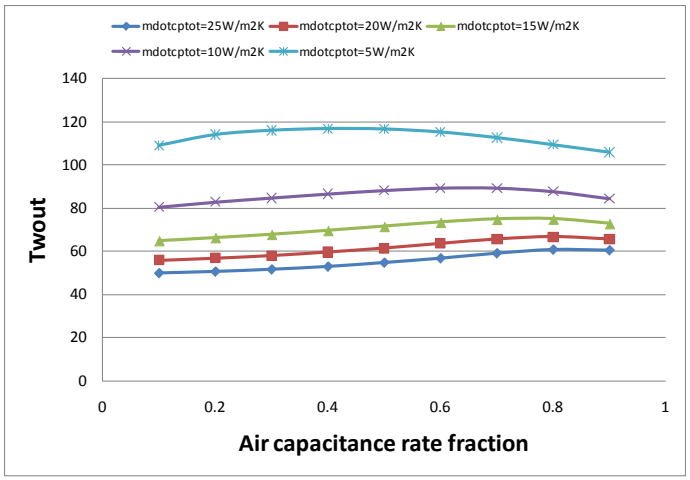

Figure 5: Water outlet temperature vs. $R_{\dot{m}cp}$ for range of $(\dot{m}c_p)_{total}$ with $T_{w,i}$ = T_{amb} = 25°C for uncoupled air heating.

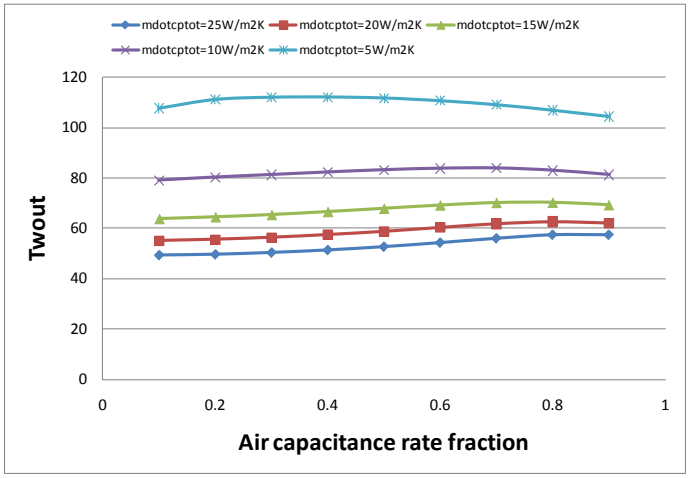

Figure 6: Water outlet temperature vs. $R_{\dot{m}cp}$ for range of $(\dot{m}c_p)_{total}$ with $T_{w,i}$ = T_{amb} = 25°C for coupled air heating.

The third analysis develops standard performance curves for the collector for a wider range of varying parameters and conditions. For this analysis $(\dot{m}c_p)_{total}$ has been kept constant at 15W/m^{2}K , while $R_{\dot{m}cp}$, V_w, T_{wi}, T_{amb} and G have been varied. The ranges of values for which these parameters have been varied are displayed in Table 2. The results from this analysis are illustrated in Figures 13 and 14 and 15 and 16 for uncoupled air heating and coupled air heating behind the collector plate.

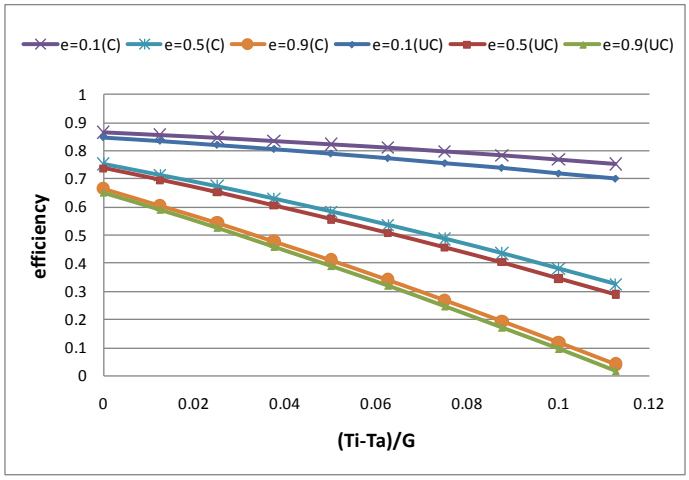

Figure 7: Efficiency vs. ΔT/G for $R_{\dot{m}cp}$= 0.1 and T_{amb} = 25°C for uncoupled (UC) and coupled(C) air heating behind plate.

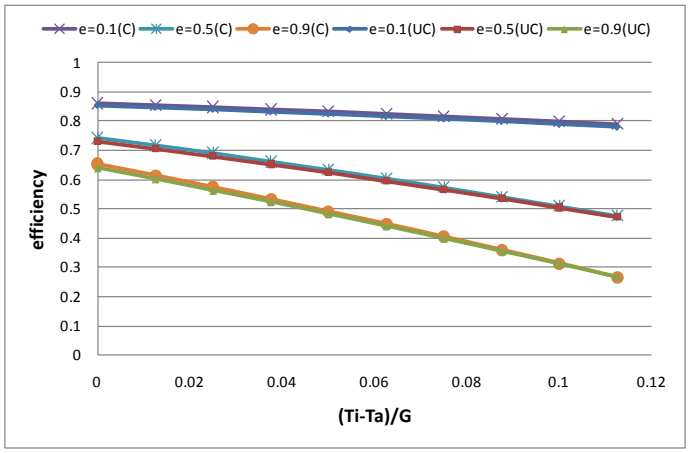

Figure 8: Efficiency vs. ΔT/G for $R_{\dot{m}cp}$= 0.5 and T_{amb} = 25°C for uncoupled (UC) and coupled(C) air heating behind plate.

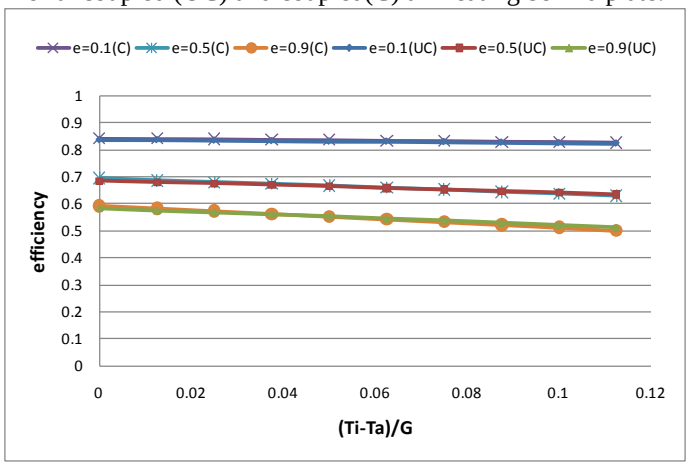

Figure 9: Efficiency vs. ΔT/G for $R_{\dot{m}cp}$= 0.9 and T_{amb} = 25°C for uncoupled (UC) and coupled(C) air heating behind plate.

Table 2: Conditions used in sensitivity analyses

Parameter	Values
(1)Air temperature(T_{amb})	25,35,45(^oC)
(1)Water inlet temperature(T_{wi})	25-115 (^oC) with 10 ^oC intervals
(1)Air to total thermal capacity ratio($\dot{m}c_{p\ ratio}$)	0.1, 0.3, 0.5, 0.7, 0.9
(2)Solar radiation (G)	300, 500, 800 (W/m^2)
(2)Wind speed(V_w)	0, 3, 5 (m/s)

(1) G and V_w are fixed for the first two sensitivity exercises at values given in Table 1.
(2) G and Vw are only varied for the standard collector performance curve plots (figures 8 &9) that show wind speed sensitivity.

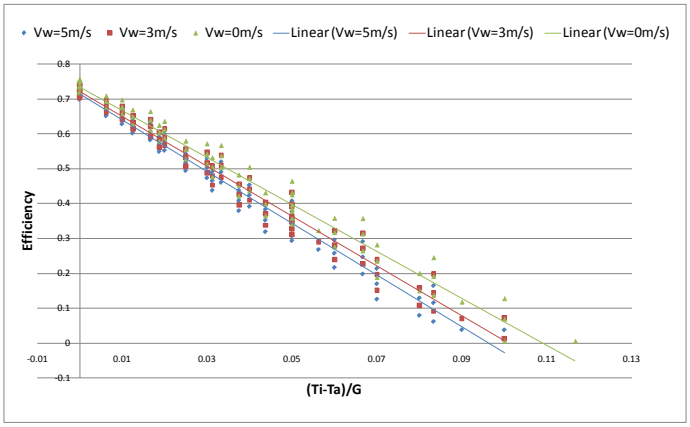

Figure 10: Efficiency vs. ΔT/G for $R_{\dot{m}cp}$= 0.1, $(\dot{m}c_p)_{total}$=15W/m^{2}K and varying G, T_{amb}, T_{win}, and V_w for uncoupled heating behind collector plate.

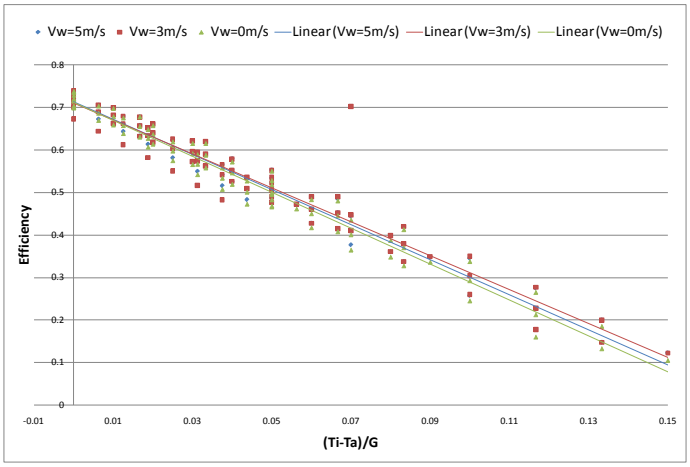

Figure 11: Efficiency vs. ΔT/G for $R_{\dot{m}cp}$= 0.5, $(\dot{m}c_p)_{total}$=15W/m^{2}K and varying G, T_{amb}, T_{win}, and V_w for uncoupled heating behind collector plate.

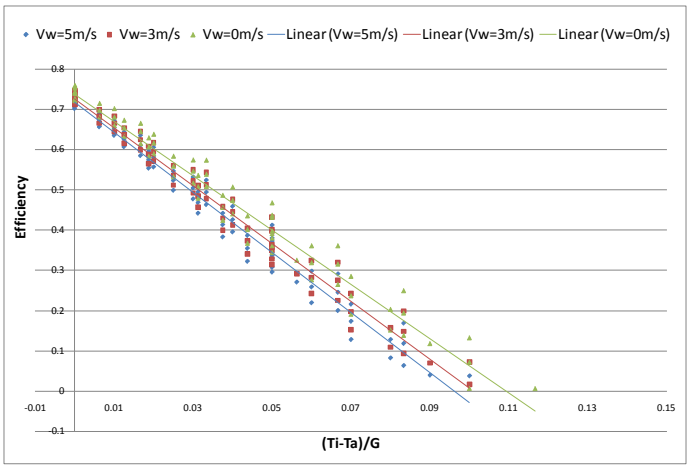

Figure 12: Efficiency vs. ΔT/G for $R_{\dot{m}cp}$= 0.1, $(\dot{m}c_p)_{total}$=15W/m^{2}K and varying G, T_{amb}, T_{win}, and V_w for coupled heating behind collector plate.

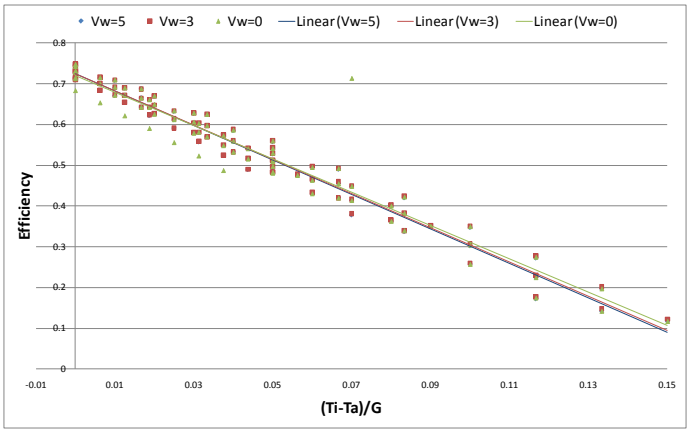

Figure 13: Efficiency vs. ΔT/G for $R_{\dot{m}cp}$= 0.5, $(\dot{m}c_p)_{total}$=15W/m^{2}K and varying G, T_{amb}, T_{win}, and V_w for coupled heating behind collector plate.

Finally the pitch and diameter of the holes was varied to assess the impact on the efficiency of the collector for the coupled model only. First the hole diameter was varied from 0.001 to 0.0055m, keeping the pitch constant at 0.025m. Then the hole diameter was kept constant at 0.00159m while the pitch was varied from 0.01 to 0.055m. This allowed for the collector performance to be simulated for a range of values of:

$$0.25< \left(\frac{pitch}{D_h}\right)^{-1.21} {Re_d}^{0.43} < 1.039$$

This range lies within the range of values for which equation (5) is valid. The analysis was performed for total capacitance rates of 30, 40 and 50W/m^{2}K, keeping the air capacitance ratio of 0.5. The results of these analyses are shown in figures 14 and 15 respectively.

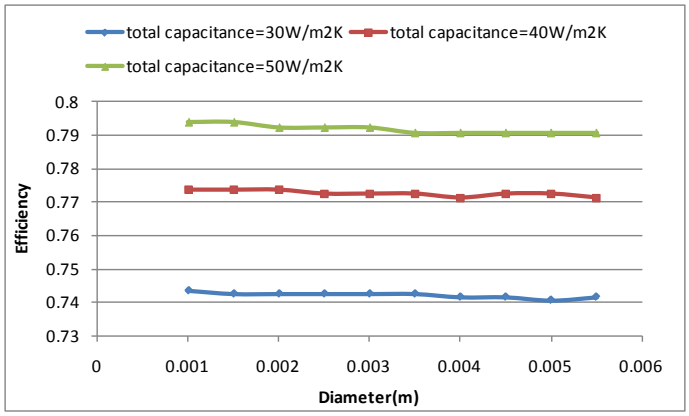

Figure 14: Efficiency vs. Hole Diameter for a constant pitch of 0.025m and air capacitance ratio of 0.5.

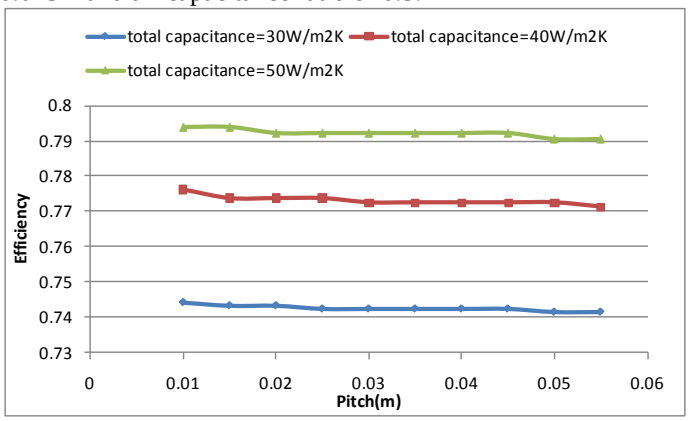

Figure 15: Efficiency vs. Pitch for a constant hole diameter of 0.00159m and air capacitance ratio of 0.5.

DISCUSSION

The results from the first sensitivity analysis show that the efficiency of the collector is highest when $R_{\dot{m}cp}$ is between 0.3 and 0.4 for both the uncoupled and coupled air heating model. It also shows the general trend of increasing efficiency with increasing$(\dot{m}c_p)_{total}$. The existence of a maximum efficiency point at an intermediate ratio of air-to-total flow rate may be attributed to the fact that as the $R_{\dot{m}cp}$ increases, the convective losses due to wind decrease, leading to an increase in the efficiency of the collector. However after a certain increase in $R_{\dot{m}cp}$, further increase in the ratio has very little effect on the convective losses. Thus as the mass flow rate of water decreases, the plate temperature increases, leading to a rapid increase in the radiative losses and, consequently, a decrease in collector efficiency.

As expected the collector is more efficient overall when heating of air behind the plate is promoted rather than suppressed. However the efficiency difference is not large as seen in figures 3 and 4. This means that if we design to suppress convective coupling behind the plate (e.g by using a denser pattern of smaller holes), the collector can be accurately modeled using the uncoupled model. One reason to suppress convection is to heat the water preferentially for the desiccant regeneration application.

The second sensitivity analysis shows the trend of decreasing efficiency of the collector for all three $R_{\dot{m}cp}$ of 0.1, 0.5 and 0.9 as $(T_i\text{-}T_{amb})/G$ is increased (Figures 7-12). One trend worth noticing is that as the $R_{\dot{m}cp}$ is increased, the decrease in efficiency with increasing $(T_i\text{-}T_{amb})/G$ is less steep. This can be attributed to the increased heat transfer to the air at the higher water inlet temperatures, corresponding to low plate temperatures, which allows the collector to maintain a high efficiency at high inlet temperatures.

The results from the third sensitivity analysis show that there is a general trend of decrease in the efficiency of the collector as $\Delta T/G$ is increased. The trend is highlighted by adding a line of best fit to the results obtained from the analysis. Furthermore it may be seen that when $R_{\dot{m}cp}$ is low (Figure 8), the efficiency of the collector is sensitive to the wind speed. This phenomenon may be explained by the fact that at a low $R_{\dot{m}cp}$, the convective losses from the collector are weakly suppressed and thus an increase in the wind speed increases the convective losses, hence decreasing the collector efficiency. Thus it may be observed that the LATSC behaves similar to a glazed collector at moderate to high air capacitance ratios. The designer must be mindful of local wind conditions when applying the same generalization to lower air capacitance ratios.

From the last sensitivity analysis, it may be seen that there is a general, but small, reduction in the efficiency of the collector with increase in pitch and hole diameter. Thus the efficiency of the collector is insensitive to changes in the pitch and diameter for low porosity absorber plates.

FUTURE WORK

The next step in the study of the LATSC is experimental validation of the model. In this regard, a test rig based on a $2m^2$ collector has been assembled at MIST.
In addition to experimental verification a system model is being developed which integrates the LATSC and a liquid desiccant regeneration system to assess the performance of the regenerator coupled with the LATSC model. If the air flow ratio can be adjusted with relatively small adverse impact on the regeneration process, there is clearly an opportunity to maintain high overall efficiencies over a range of conditions by proper balancing of the air and water flow rates. The LATSC model must be linked to a regeneration process model for the control problem to be properly addressed.
In addition to the flow balance control problem, the opportunity to improve system performance by adjusting the distribution of collector plate porosity in the flow direction, currently modeled such that uniform face velocity is achieved, may be explored.

CONCLUSION

A numerical model of a novel hybrid liquid air collector has been developed and the outlet water and air temperatures are evaluated by solving a system of ODEs. Two parallel models are run with fully coupled heat transfer to the air behind the collector plate and the other with no heat transfer to the air behind the collector plate. The latter is shown to reduce to the Hottel-Whillier equation. Key parameters of the model have been varied to assess the impact on the performance of the collector.

Increasing the $(\dot{m}c_p)_{total}$ increases the efficiency of the collector for all values of $R_{\dot{m}cp}$. Moreover, an increase of the $R_{\dot{m}cp}$ from 0.1 to about 0.4 at a constant $(\dot{m}c_p)_{total}$ has shown to increase the efficiency of the collector while further increase in $R_{\dot{m}cp}$ has leads to a decrease in the efficiency because of higher plate temperatures near the outlet ends of the tubes. Furthermore, although an increase of $(T_i-T_{amb})/G$ always decreases the efficiency of the collector for $R_{\dot{m}cp}$ of 0.1, 0.5 and 0.9, the rate of decrease of the efficiency decreases with an increase in $R_{\dot{m}cp}$. For a low $R_{\dot{m}cp}$ of 0.1, the efficiency of the collector exhibitss considerable sensitivity to wind speed, showing that the convective losses are only marginally suppressed at low air flow rates. To heat the cooling water preferentially while still providing enough airflow to suppress convective front losses, it is desirable to conduct the air through the plate and into the airstream behind the plate in such a way that convective coupling is minimized.

REFERENCES

1. Ali, M.T., et al., *A Cooling Change-Point Model of Community-Aggregate Electrical Load.* Energy and Buildings, 2011. **43**: p. 28-37.
2. Remund, J., R. Lang, and S. Kunz, *METEONORM*. 2003, Meteotest: Bern, Switzerland.
3. Threlkeld, J.L., J.W. Ramsey, and T.H. Kuehn, *Thermal Environmental Engineering*. Third Edition. 1998: Prentice-Hall.
4. Armstrong, P.R., et al., *Efficient Low-Lift Cooling with Radiant Distribution, Thermal Storage, and Variable-Speed Chiller Controls— Part I: Component and Subsystem Models.* HVAC&R RESEARCH, 2009. **15**(2): p. 366-400.
5. H.M Henning, T.E., C. Hindenburg, I.S. Santamaria, *The potential for solar energy use in desiccant cooling cycles* International Journal of Refrigeration, 2001. **24**: p. 220-229.
6. Pesaran, A.A. and K. Wipke, *Desiccant Cooling Using Unglazed Transpired Solar Collectors*, in *Solar '92*, S.M. Burley and M.E. Arden, Editors. 1992, American Solar Energy Society: Cocoa Beach Flordia.
7. Kutscher, C.F., C.B. Christensen, and G.M. Barker, *Unglazed Transpired Solar Collectors: Heat Loss Theory.* Journal of Solar Energy Engineering, 1993. **115**(3): p. 182-188.
8. Kutscher, C.F., *Heat Exchange Effectiveness and Pressure Drop for Air Flow Through Perforated Plates With and Without Crosswind.* Journal of Heat Transfer, 1994. **116**(2): p. 391-399.
9. Duffie, J. and W. Beckman, *Solar Engineering of Thermal Processes*. 1980: John Wiley & Sons Inc.
10. Incropera, et al., *Fundamentals of Heat and Mass Transfer*. 2006: Wiley.
11. *MATLAB*. 2008, The MathWorks, Inc.

APPENDIX:

Linearized Model:

We observed that the LATSC model with heat transfer to the air behind the absorber plate gives performance not much different from that given by the model with no heat transfer behind the absorber plate. These observations suggest a simplified model based on the Hottel-Whillier(H-W) equation. In this case, for negligible back loss to ambient, the water heating is given by:

$$Q_u = W * dy * \left(F_R G - U_l\left(T_{fi} - T_{amb}\right)\right) \quad (24)$$

Where:

$$F_R = \frac{\dot{m}_w c_{pw}}{A_c U_l F'}\left(1 - \exp\left(-\frac{A_c U_l F'}{\dot{m}_w c_{pw}}\right)\right) \quad (25)$$

F_R is the heat removal factor of the plate and it is the ratio of the total heat transferred to the water to the energy that would be transferred if the plate temperature was equal to the fluid inlet temperature.

The H-W formulation requires a constant radiation heat transfer coefficient (h_r) with the sky temperature, T_{sky}, assumed to be equal to ambient temperature T_{amb}. Therefore equations 12 and 13 are changed to:

$$q_{rad,loss} = \epsilon\sigma 4{T_m}^3(T_{pl} - T_{amb}) \quad (26)$$

Where

$$T_m = (T_{pl} + T_{amb})/2 \quad (27)$$

The radiation heat transfer coefficient of the plate can then be expressed as:

$$h_r = \epsilon\sigma 4{T_m}^3 \quad (28)$$

While the convective heat transfer coefficients due to wind and suction through the plate can be expressed as:

$$h_{wind} = 0.82\frac{V_w \mu_a \rho_a c_{pa} k_a}{V_s L L_c} \quad (29)$$

$$h_{c,air} = \dot{m}_a c_{pa} e_{hx} \quad (30)$$

The total heat loss coefficient from the plate is the sum of the three transfer coefficients:

$$U_l = h_r + h_{wind} + h_{c,air} \quad (31)$$

Moreover the air heating is given by:

$$q_{c,air} = \dot{m}_a c_{pa} e_{hx}(T_{pm} - T_{amb}) \quad (32)$$

Where $$T_{pm} = T_{fi} + \frac{Q_u}{A_c F_R U_l}(1 - F_R) \quad (33)$$

The H-W model and the uncoupled form of the numerical model were simulated using identical inlet and ambient conditions and the results showed that both the air and water outlet temperatures match within the precision of MATLAB's numerical integrator ODE45.

Given reasonable initial estimates of h_r, h_{wind} and $h_{suction}$, one can expect to obtain an accurate estimate of T_{pm} and overall collector performance in two iterations.